Ultrasonics - Sonochemistry 54 (2019) 99–109

Contents lists available at ScienceDirect

Ultrasonics - Sonochemistry

journal homepage: www.elsevier.com/locate/ultson

A simple method to analyze the super-harmonic and ultra-harmonic behavior of the acoustically excited bubble oscillator

A.J. Sojahrood[a,b,*], D. Wegierak[a,b], H. Haghi[a,b], R. Karshfian[a,b], Michael C. Kolios[a,b]

[a] Department of Physics, Ryerson University, Toronto, Canada
[b] Institute for Biomedical Engineering, Science and Technology (IBEST) a partnership between Ryerson University and St. Mike's Hospital, Toronto, Ontario, Canada

ABSTRACT

The bubble oscillator is a highly nonlinear system, which makes it difficult to generate a comprehensive understanding of its oscillatory behavior. One method used to investigate such complex dynamical systems is the bifurcation analysis. Numerous investigations have employed the method of bifurcation diagrams to study the effect of different control parameters on the bubble behavior. These studies, however, focused mainly on investigating the subharmonic (SH) and chaotic oscillations of the bubbles. Super-harmonic (SuH) and ultra-harmonic (UH) bubble oscillations remain under-investigated. One reason is that the conventional method used for generating bifurcation diagrams cannot reliably identify features that are responsible for the identification of SuH and UH oscillations. Additionally, the conventional method cannot distinguish between the UHs and SHs. We introduce a simple procedure to address this shortcoming. In this method, the maxima of the bubble oscillatory response were selected and plotted alongside the traditional bifurcation points for the corresponding control parameter. Results show that depending on the control parameters the conventional method or the method of maxima may miss intricate details of the oscillations. In order to have a comprehensive knowledge on the rich dynamics of the system, the two methods should be employed side by side. Through plotting the two bifurcation structures in tandem, the oscillatory behavior of the bubble was analyzed with more detail, and stable SuH and UH bubble oscillations were investigated. Based on this new analysis, the conditions for the generation and amplification of UH and SuH regimes are discussed.

1. Introduction

The acoustic bubble [1–12] oscillator is present in many physical phenomena and applications. Bubbles are involved in physical phenomena associated with underwater acoustics and oceanography [2,12]. Bubbles are used as catalysts for chemical reactions in sonochemistry [13–16] and several non-chemical cleaning applications [17]. Bubble oscillations drive sonoluminscence [15], and are the basis of several medical applications including, but not limited to, blood vessel imaging and treatment monitoring [18,19], drug delivery [20], blood brain barrier opening [21], high intensity focused ultrasound [22], shock wave lithotripsy [23] and histotripsy and clot lysis [24].

The bubble oscillator is a highly nonlinear dynamical system [1–12,25–41]; the oscillatory bubble behavior has been referred to as chaotic and complex [1–12,25–41]. Due to the complex behavior, a comprehensive understanding of the phenomena associated with bubble dynamics is difficult. Consequently, the optimization of applications is a challenging task. Moreover, due to the incomplete knowledge on the nonlinear behavior of bubbles, many applications are not optimized and this limits progress in the associated fields (e.g., enhanced drug delivery [20]).

Methods of nonlinear dynamics (e.g. resonance curves and bifurcation diagrams) have been extensively applied to investigate bubble behavior [1–7,25–41]. It has been shown that the bubble oscillator can exhibit $\frac{1}{2}$, $\frac{1}{3}$, $\frac{1}{4}$, $\frac{1}{5}$ or higher order SHs, as well as period doubling route to chaos [1–7,25–41]. These studies have shed light on the nonlinear dynamics and bifurcation structure of the bubbles; however, the approaches used in these publications have provided insights primarily on SH and chaotic bubble oscillations.

Recently the dynamics of a 0.1 mm gas bubble immersed in glycerine with varying temperature was studied in [42–44] where the effect of high viscosity on the bubble dynamics and the evolution of the harmonic and UH resonances were presented. Results of these studies have emphasized that knowledge of the oscillatory behavior of the bubble (including SHs and UHs) is necessary to optimize the bubble applications.

Despite many investigations of the nonlinear behavior of acoustically excited bubbles using the methods of chaos physics and nonlinear dynamics, details of the super-harmonic (SuH) and ultra-harmonic (UH) oscillations including the characteristics of the radial oscillation, phase portraits and the backscattered pressure have received less attention. The conventional analysis method only extracts the data after every period of acoustic driving pressure [1,5]. The alternative method of bifurcation analysis which is based on analyzing the peaks of the radial oscillations (e.g. employed in [25–28,38]) can not by itself produce information to help identify the SuH and/or UH behavior of the

* Corresponding author at: Department of Physics, Ryerson University, Toronto, Canada.
E-mail address: amin.jafarisojahrood@ryerson.ca (A.J. Sojahrood).

https://doi.org/10.1016/j.ultsonch.2019.02.010
Received 20 September 2018; Received in revised form 19 January 2019; Accepted 11 February 2019
Available online 13 February 2019
1350-4177/

bubble.Thus, analysis methods need to be developed to identify and explore SuH and UH oscillations alongside the SH and chaotic regimes.

In this work, we introduce a more comprehensive and simple method to study the SuH and UH bubble oscillations. The bifurcation structure of the bubble oscillator is constructed using the two well-known methods in tandem. This is done by plotting the maxima of the stable oscillations of the bubble alongside the conventional bifurcation points at each corresponding control parameters in the bifurcation diagrams. Through plotting the two bifurcation curves we were able to straightforwardly identify the SuH and UH oscillations and explore the conditions that are required to generate and amplify the SuH and UH oscillations.This method establishes a framework that provides a more comprehensive understanding of the rich nonlinear behavior of bubbles; consequently, it may help in optimizing current applications and/or can be used to discover new nonlinear bubble behaviors that may result in new applications.

2. Methods

2.1. The Bubble model

The radial oscillations of the bubbles are numerically simulated by solving the well known Keller-Miksis equation [45]:

$$\rho\left(1-\frac{\dot{R}}{c}\right)R\ddot{R}+\frac{3}{2}\rho\dot{R}^2\left(1-\frac{\dot{R}}{3c}\right)=\left(1+\frac{\dot{R}}{c}+\frac{R}{c}\frac{d}{dt}\right)\left((p_0+\frac{2\sigma}{R_0})\left(\frac{R_0}{R}\right)^{3k}-\frac{2\sigma}{R}-\frac{4\mu\dot{R}}{R}-P_0+P_A sin(2\pi ft)\right) \quad (1)$$

In this equation, R is radius at time t, R_0 is the initial bubble radius, $\dot{R}$ is the wall velocity of the bubble and $\ddot{R}$ is the wall acceleration ρ is the liquid density $\left(998\ \frac{kg}{m^3}\right)$, c is the sound speed (1481 m/s), P_0 is the atmospheric pressure (101 kPa), σ is the surface tension $\left(0.0725\ \frac{N}{m}\right)$, μ is the liquid viscosity (0.001 Pa·s), P_A and f are the amplitude and frequency of the applied acoustic pressure. The values in the parentheses are for water at 293 ^{0}K and are used in all the simulations. The gas inside the bubble is air with polytropic exponent of k = 1.4.

Oscillations of a bubble generates a backscattered pressure (P_{Sc}) which can be calculated by [46]:

$$P_{Sc}=\rho\left(\frac{R}{d}\right)(R\ddot{R}+2\dot{R}^2) \quad (2)$$

where d is the distance from the center of the bubble (and for simplicity is considered as 1 m in this paper) [46].Backscattered pressure is directly related to the radial oscillations of the bubble but is a more complex function of the radial oscillations and also will be affected by the frequency dependent attenuation in tissue [47]. Calculation of the backscattered pressure is of great importance since in several applications the backscattered pressure resulting from bubble oscillations plays a critical role. For example, in imaging applications the backscattered pressure is detected and analyzed to form images. In shock wave lithotripsy the backscattered pressure is used to break and disintegrate kidney stones. In majority of the applications and phenomena involving bubble dynamics, monitoring the behavior of the bubbles is through recording the backscatterd signal and analyzing its frequency components.

Eq. (1) is solved using the 4th order Runge–Kutta technique (with an embeded 5th order error estimation); the control parameters of interest are R_0, $f$and P_A. The resulting radial bubble oscillations are visualized using the bifurcations diagrams. The simulations were done using the ode45 function of MATLAB and the relative and absolute tolerance of the integration was set to 1e−12 and 1e−13. The solutions were recorded at time steps of $\frac{0.001}{f}$. The initial conditions of the problem were set to $R_0(t=0)=R_0$ and $\dot{R}(t=0)=0$ m/s. Bifurcation diagrams of the normalized bubble oscillations $\frac{R}{R_0}$ are presented as a function of driving pressure. Detailed analysis is presented at select control parameters using a) the radius versus time curves, b) phase portrait analysis and c) the frequency spectrum of the backscattered pressure.

2.2. Bifurcation diagrams

For highly nonlinear systems like bubble oscillators, small changes in the initial conditions of the system or control parameters can result in large changes in the behavior of the system. Due to the complexity and sensitivity of the bubble dynamics to the exposure parameters (frequency and acoustic pressure) and the initial conditions, a comprehensive understanding of the bubble dynamics is a challenging task and requires investigation of the behavior of the system over a wide range of the control parameters. Bifurcation diagrams are valuable tools to analyze the dynamics of nonlinear systems where the qualitative and quantitative changes of the dynamics of the system can be investigated effectively over a wide range of the control parameters.

2.2.1. Conventional bifurcation analysis

When dealing with systems responding to a driving force, to generate the points in the bifurcation diagrams vs. the control parameter, one option is to sample from a specific point in each driving period. The approach can be summarized in:

$$Q\equiv(R(\Theta))\left\{(R(t),\dot{R}(t)):\Theta=\frac{n}{f}\right\}\quad where\quad n=100,\ 101...150 \quad (3)$$

where Q denotes the points in the bifurcation diagram, R and $\dot{R}$ are the time dependentradius and wall velocity of the bubble at a given set of control parameters of $(R_0,\ P_0,\ P_A,\ c,\ k,\ \mu\,\sigma, f)$ and Θ is given by $\frac{n}{f}$. Points on the bifurcation diagram are constructed by plotting the solution of $R(t)$ at time points that are multiples of the driving acoustic period. The results are plotted for n = 100–150 to ensure a steady state solution has been reached.

2.2.2. Method of peaks

As a more general method, bifurcation points can be constructed by setting one of the phase space coordinates to zero:

$$Q\equiv max(R)\{(R,\dot{R}):\dot{R}=0\} \quad (4)$$

In this method, the steady state solution of the radial oscillations for each control parameter is considered. The maxima of the radial peaks ($\dot{R}=0$) are identified (determined within 100–150 cycles of the stable oscillations) and are plotted versus the given control parameter in the bifurcation diagrams. The bifurcation diagrams of the normalized bubble oscillations $\left(\frac{R}{R_0}\right)$ are calculated using both methods a) and b). When the two results are plotted alongside each other, it is easier to uncover more important details about the SuH and UH oscillations, as well as the SH and chaotic oscillations.

3. Results

To illustrate how the method of constructing the bifurcation diagram can influence the classification of the oscillatory patterns, we have considered a bubble with initial diameter of 4 microns. The linear resonance frequency (f_r) of the bubble is ~2.04 MHz. f_r is calculated by numerically solving Eq. (1) for P_A = 1 kPa and finding the frequency that results in the maximum expansion ratio. We have studied the bifurcation structure of the bubble in the form of $\frac{R}{R_0}$ as a function of the driving acoustic pressure for (400 kHz < f < 6 MHz) and (1 kPa < P_A < 3 MPa). For simplicity we focus on the stable non-destructive regime of oscillations and results are only presented for pressure ranges that leads to radial oscillations with $\frac{R}{R_0}\leqq 2$ [27].

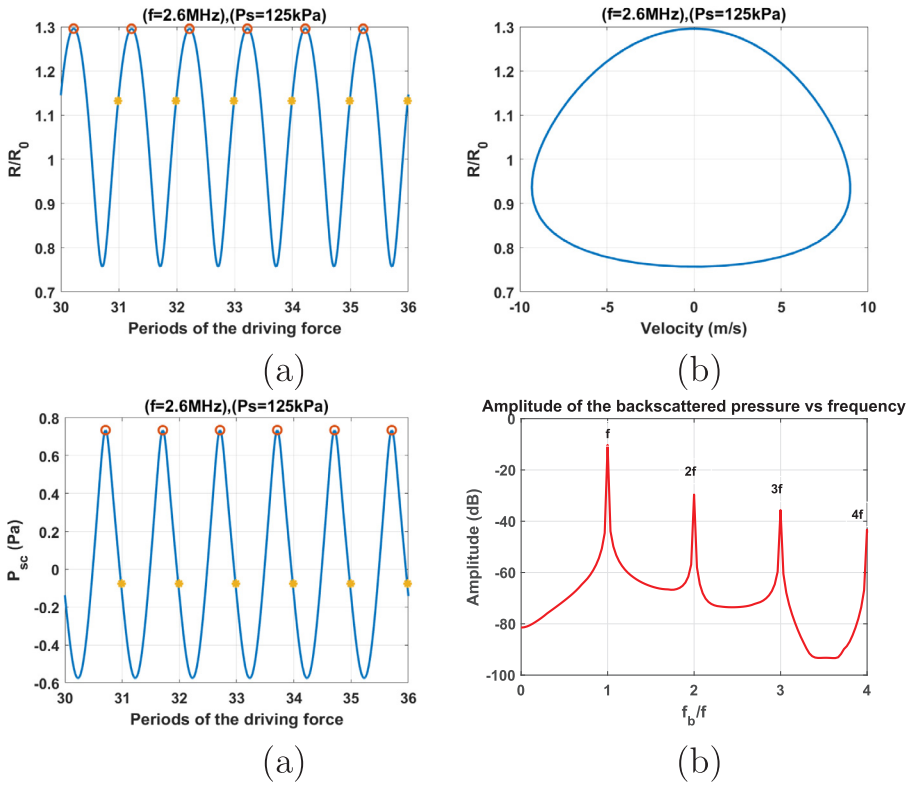

Fig. 1. Oscillation characteristics of a 4 micron bubble driven at f = 2.6 MHz and 125 kPa of pressure: a) Radial oscillations versus driving periods. Yellow dots correspond to R(t) values at each period (conventional method) and Red dots (peaks method) are positioned at the peaks of the R(t) curve. b) phase portrait diagrams c) Backscattered pressure a and d) frequency spectrum of the backscattered pressure. (For interpretation of the references to colour in this figure legend, the reader is referred to the web version of this article.)

3.1. Example of SHs, UHs and SuHs oscillations

To gain a better insight of the oscillation characteristics that the conventional bifurcation analysis method will be unable to reveal, first we will show different regime of oscillations in detail. In this regard a) radial oscillations vs. driving acoustic periods, b) phase portraits, c) backscattered pressure vs. driving periods and d) backscattered frequency spectra are examined in detail. Exposure parameters relevant to biomedical applications were chosen. Fig. 1a depicts the radial oscillations of the bubble for P_A = 125 kPa and f = 2.6 MHz. The yellow stars represent the amplitude of radial oscillations after every period, and the red circle illustrates the maxima of the curve. There exists only one value for all red circles and yellow stars; therefore, the behavior is a period-1 (P1) signal with one maximum. In this case both methods predict the same behavior. The corresponding phase portrait in Fig. 1b is a semi circular orbit with one loop. The backscattered pressure has one peak and is shown in Fig. 1c and the corresponding fundamental component of the P_{Sc} in Fig. 1d is stronger than the SuHs.

Fig. 2a shows the R-T curve that corresponds to P_A = 78 kPa and f = 1.2 MHz. The signal has two maxima, while the amplitude of the signal at each driving period remains the same. In this case the two methods do not provide the same results. This suggests a P1 signal with two maxima. Fig. 2b shows that the phase portrait of the bubble undergoes an internal bend; depicting a similar behavior when SHs are present in the curve. However, the absence of SHs are evident in the frequency spectra (Fig. 2d) of the corresponding P_{Sc} shown in Fig. 2c while the 2nd harmonic has the highest value (2nd harmonic resonance). In this case examination of the maxima provides more complete information about the oscillation characteristics, identifying a 2nd SuH resonance.

Figs. 3 and 4 compare the characteristics of two P2 oscillations; one has two maxima while the other has 4 maxima. Fig. 3a shows the R-T curve of the bubble for f = 2.6 MHz and P_A = 275 kPa. The signal has two maxima (two red dots), and the signal repeats its pattern once every two acoustic driving periods (two yellow stars). The phase portrait (Fig. 3b) consists of two circular orbits with one creating another and enclosing it within itself. The backscattered pressure is shown in Fig. 3c and has 2 maxima. Fig. 3d depicts the existence of $\frac{1}{2}$ order SH which is stronger than the UH components. Fig. 4a shows the R-T curve of the bubble for f = 1.2 MHz and P_A = 145 kPa; the signal is of P2 but with 4 distinct maxima. The radial oscillations repeat their pattern once every two acoustic periods (two yellow stars), and each pattern has 4 maxima (4 red dots). The phase portrait has two circular orbits similar to Fig. 3b; however, each of these circular orbits underwent an internal bend. The backscattered pressure is shown in Fig. 4c and has 4 maxima. The frequency content of the P_{Sc} in Fig. 4f has $\frac{1}{2}$ order SHs as well as UHs; the 2nd order SuH is the strongest signal, and $\frac{5}{2}$ and $\frac{7}{2}$ UHs are stronger than $\frac{1}{2}$ order SH and other UHs.

Fig. 5a shows the R-T curve that corresponds to P_A = 135 kPa and f = 4.068 MHz. The signal has only one maxima, while the amplitude of the signal at each driving period has two distinct values. This suggests a P2 signal with one maximum. Fig. 5b shows that the phase portrait of the bubble consists of rotated semi heart shape loop. The corresponding backscattered pressure has two maxima (Fig. 5c) and the frequency component of the P_{Sc} (Fig. 5d) has a very strong SH near the fundamental level while the 2nd SuH and $\frac{3}{2}$ order UH are relatively weaker. This is an example of a case that the method of peaks fails to capture intricate details of the oscillations however the conventional method reveals the $\frac{1}{2}$ order SH resonance clearly.

Fig. 6 is another example in which the method of peaks can not capture the nature of oscillations clearly however the conventional method captures the details that the peaks method missed. Fig. 6a shows the R-T curve that corresponds to P_A = 400 kPa and f = 5.8986 MHz. The signal has only one maxima, while the amplitude of the signal at each driving period has three distinct values. This suggests a P3 signal with one maximum. Fig. 6b shows that the phase portrait of the bubble consists of a duck shape loop. The corresponding backscattered pressure has three maxima (Fig. 6c) and the frequency component of the signal has a very strong $\frac{1}{3}$ and $\frac{2}{3}$ SH near the fundamental level while the 2nd SuH and other UHs and SHs are relatively weaker.

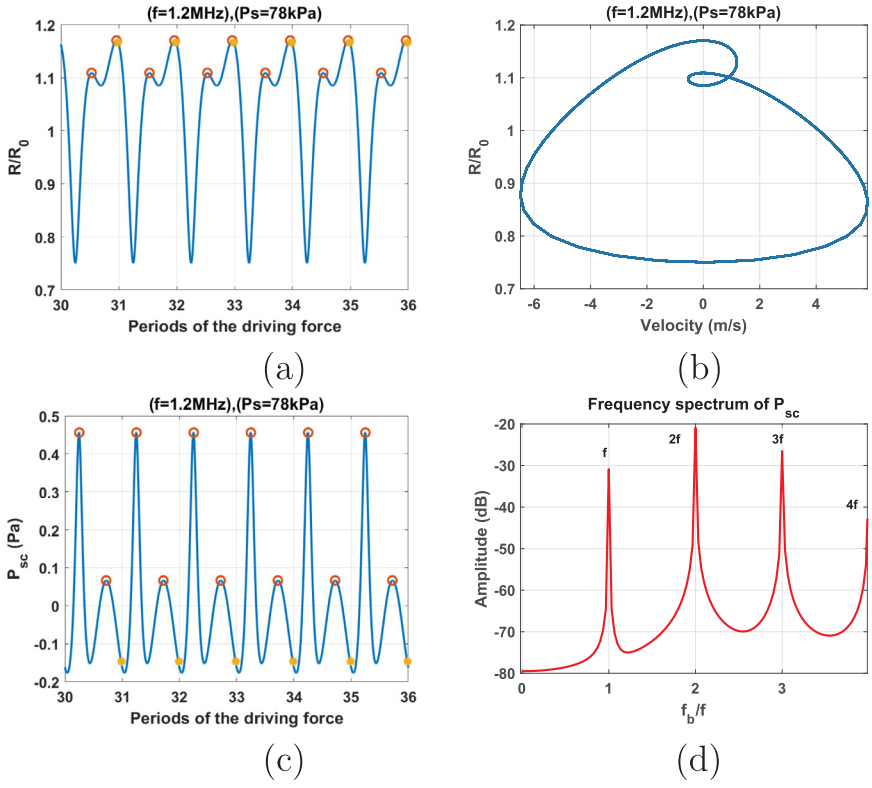

Fig. 2. Oscillation characteristics of a 4 micron bubble driven at f = 1.2 MHz and 78 kPa of pressure: a) Radial oscillations versus driving periods. Yellow dots correspond to R(t) values at each period (conventional method) and Red dots (peaks method) are positioned at the peaks of the R(t) curve. b) phase portrait diagrams c) Backscattered pressure a and d) frequency spectrum of the backscattered pressure. (For interpretation of the references to colour in this figure legend, the reader is referred to the web version of this article.)

3.2. Bifurcation diagrams and power spectrum

After introducing a few examples in Figs. 1–6 here we examine the bifurcation structure of the $\frac{R}{R_0}$ of bubble as a function of pressure that is constructed by the two methods in tandem. The frequency components of the backscattered pressure are also plotted along side the bifurcation diagrams to visualize the evolution of the frequency spectra as pressure increases. To focus on more practical and stable oscillation regimes, we have omitted the parameter ranges that result in chaotic oscillations or bubble destruction $\left(\frac{R}{R_0} > 2\right)$. As it is discussed in detail in [16], $\frac{R}{R_0} > 2$ seems to be the minimum estimated expansion ratio for bubble destruction. The bifurcation structures that are produced using the

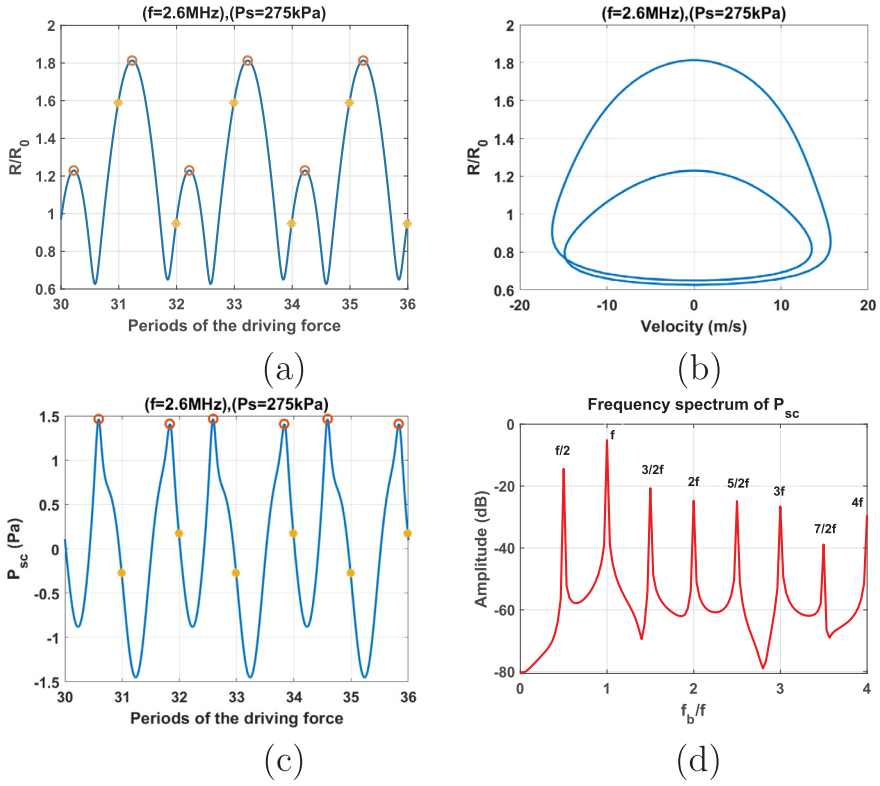

Fig. 3. Oscillation characteristics of a 4 micron bubble driven at f = 2.6 MHz and 275 kPa of pressure: a) Radial oscillations versus driving periods. Yellow dots correspond to R(t) values at each period (conventional method) and Red dots (peaks method) are positioned at the peaks of the R(t) curve. b) phase portrait diagrams c) Backscattered pressure a and d) frequency spectrum of the backscattered pressure. (For interpretation of the references to colour in this figure legend, the reader is referred to the web version of this article.)

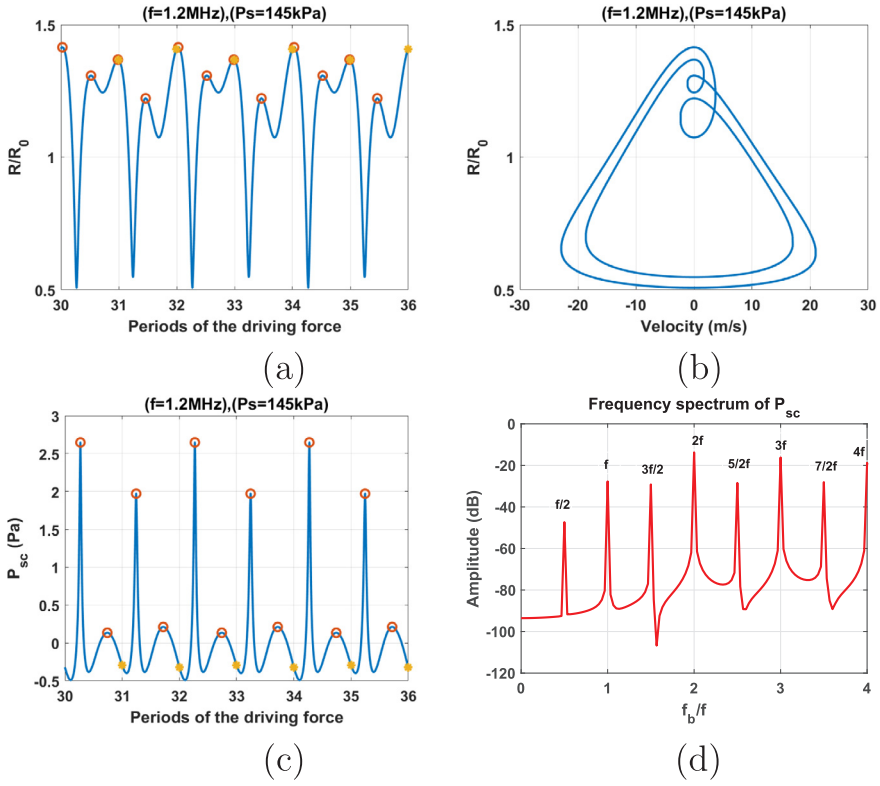

Fig. 4. Oscillation characteristics of a 4 micron bubble driven at f = 1.2 MHz and 145 kPa of pressure: a) Radial oscillations versus driving periods. Yellow dots correspond to R(t) values at each period (conventional method) and Red dots (peaks method) are positioned at the peaks of the R(t) curve. b) phase portrait diagrams c) Backscattered pressure a and d) frequency spectrum of the backscattered pressure. (For interpretation of the references to colour in this figure legend, the reader is referred to the web version of this article.)

conventional method are presented in blue, and the ones produced by the method of peaks are shown in red. Results are shown in Figs. 7–11.

Fig. 7a shows the response of the bubble when f = 0.7 MHz. The conventional method reveals a period 1 solution for P_A < 118 kPa and detects the generation of period 2 solution for P_A > 120 kPa. On the other hand, the peaks method reveals the generation of two maxima at 24 kPa < P_A < 56 kPa and three maxima for 56 kPa < P_A < 118 kPa. The three maxima undergo period doublings (PDs) resulting in a solution with 6 maxima for P_A > 118 kPa.

Examination of the frequency content of the backscattered pressure reveals the underlying phenomenon which results in the discrepancy between the two methods. Fig. 7b shows the amplitude of the

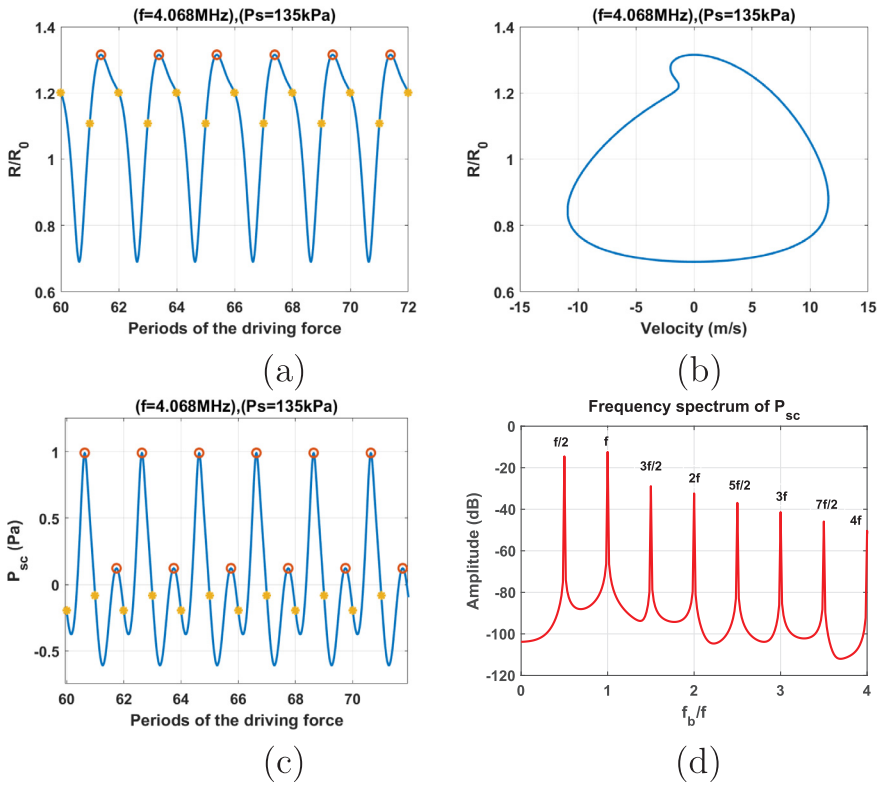

Fig. 5. Oscillation characteristics of a 4 micron bubble driven at f = 4.068 MHz and 135 kPa of pressure: a) Radial oscillations versus driving periods. Yellow dots correspond to R(t) values at each period (conventional method) and Red dots (peaks method) are positioned at the peaks of the R(t) curve. b) phase portrait diagrams c) Backscattered pressure a and d) frequency spectrum of the backscattered pressure. (For interpretation of the references to colour in this figure legend, the reader is referred to the web version of this article.)

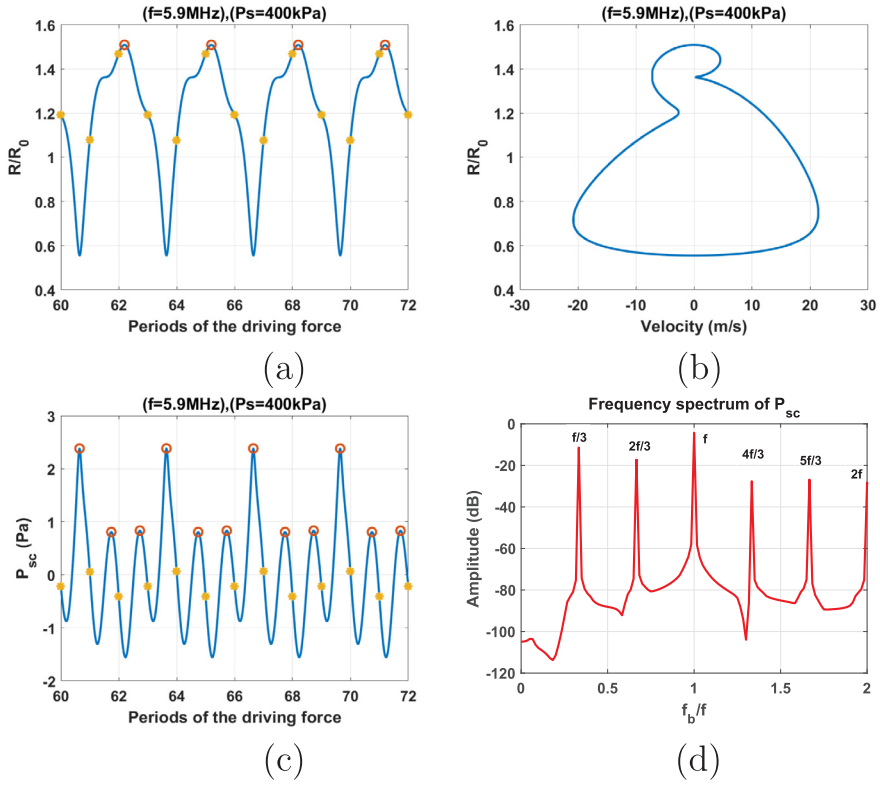

Fig. 6. Oscillation characteristics of a 4 micron bubble driven at f = 5.9 MHz and 400 kPa of pressure: a) Radial oscillations versus driving periods. Yellow dots correspond to R(t) values at each period (conventional method) and Red dots (peaks method) are positioned at the peaks of the R(t) curve. b) phase portrait diagrams c) Backscattered pressure a and d) frequency spectrum of the backscattered pressure. (For interpretation of the references to colour in this figure legend, the reader is referred to the web version of this article.)

harmonics and UHs of the backscattered signal. The occurrence of the maxima correlates with the resonance of the harmonic contents of the signal. After a pressure threshold (~25 kPa), the 3rd SuH of the backscattered signal becomes stronger than the fundamental and other SuH harmonics, showing a 3rd SuH resonance. The 3rd SuH saturates for $P_A > 56$ kPa concomitant with the occurrence of 3 maxima in the peaks methods. The SH and UH contents of the backscattered signal are shown in Fig. 7c. The simultaneous appearance of period doublings (PDs) in the blue curve and multiple PDs in the red curve are coincident with a sharp increase in the SH and UH content of the backscattered signal (Fig. 7c, arrow); the backscatter at the $\frac{7}{2}$ (purple) and $\frac{9}{2}$ UHs (green) are the strongest whit the $\frac{1}{2}$ SH (blue) the weakest component.

Fig. 8a shows that when sonication frequency is 1.2 MHz the conventional method depicts a similar behavior to f = 0.7 MHz (Fig. 1a); a linear response is observed for $P_A < 110$ kPa and radial oscillations undergo a PD for $P_A > 110$ kPa. The method of peaks reveals a solution with one maximum for PA<51 kPa which is similar to the conventional method; above this pressure, however, 2 maxima occur in the bifurcation diagram up until $P_A = 110$ kPa which are not detected in the conventional method. For PA>110 kPa, the oscillations undergo two concomitant PDs resulting in a solution with 4 maxima. The conventional method predicted the same behavior for the two frequencies (0.7 MHz (Fig. 7a) and 1.2 MHz (Fig. 8a)), however, the method of peaks revealed more intricate details of the bubble dynamics. Fig. 8b shows that the second harmonic of the backscattered signal has the strongest amplitude and saturates concomitant with the generation of the initial two maxima at ~52 kPa. Fig. 8c illustrates a sharp increase in the amplitude of SH and UHs concomitant with the generation of PDs (arrow) in the blue and red curves as shown in Fig. 1b. UH components of the signal are stronger than the SHs (~20 dB) with $\frac{5}{2}$ and $\frac{3}{2}$ UHs being the strongest while the $\frac{1}{2}$ SH is the weakest component.

Fig. 9a shows that when f = 2.6 MHz the conventional method (blue) and method of peaks (red) depict a similar behavior to f = 0.7 MHz and f = 1.2 MHz (Figs. 7a and 8a). The oscillations are of period 1 in both graphs until $P_A = 243$ kPa; above this pressure, PD occurs in both methods. The fundamental frequency is the strongest frequency component in the backscattered signal as is shown in Fig. 9b. Fig. 9c indicates that the SH and UH components of the signal increase rapidly at pressures at which the PD occurs in Fig. 1c; the SH component is stronger than all the UHs.

Fig. 10a shows that when f = 4.068 MHz and for P_A less than 66 kPa the conventional method (blue) and method of peaks (red) depict a similar behavior to f = 0.7 MHz,f = 1.2 MHz and f = 2.6 MHz (Figs. 7a, 8a, 9a). The oscillations are of period 1 in both graphs until $P_A = 66$ kPa; above this pressure, PD occurs in both methods. The fundamental frequency is the strongest frequency component in the backscattered signal as is shown in Fig. 10b. Fig. 10c indicates that the SH and UH components of the signal increase rapidly (shown by arrow) at pressures at which the PD occurs in Fig. 10a; the SH component is stronger than all the UHs. However, as the pressure increase above $P_A = 66$ kPa, one of the maxima disappears while the conventional method still depicts a P2 solution. In this case the maxima method fails to capture all the details of the oscillations. Above $P_A = 228$ kPa the second maxima returns and oscillations become again P2 with two maxima.

Fig. 11a shows the bifurcation structure of the $\frac{R}{R_0}$ as a function of pressure when f = 5.9 MHz. For P_A less than 370 kPa the conventional method (blue) and method of peaks (red) depict a similar behavior to f = 0.7 MHz,f = 1.2 MHz, f = 2.6 MHz and 4.068 MHz (Figs. 7a, 8a, 9a and 10a). The oscillations are of period 1 in both graphs and as soon as P_A increases above 370 kPa the oscillations undergo a saddle node bifurcation in both graphs. However, the method of peaks (red) displays a saddle node bifurcation from a solution with one maxima to higher amplitude solution with one maxima while the conventional method reveals more details by capturing a saddle node bifurcation from a P1 to a P3 solution. Thus oscillations are of P3 with one maxima. As the pressure increases a second maxima appears for P_A higher than 444 kPa. These solution undergo concomitant PD at $P_A = 626$ kPa; the red curve shows that the signal has 4 maxima while the blue curve depicts a P6 solution. At frequencies above resonance the maxima method was unable to reveal some intricate details of oscillations while for frequencies

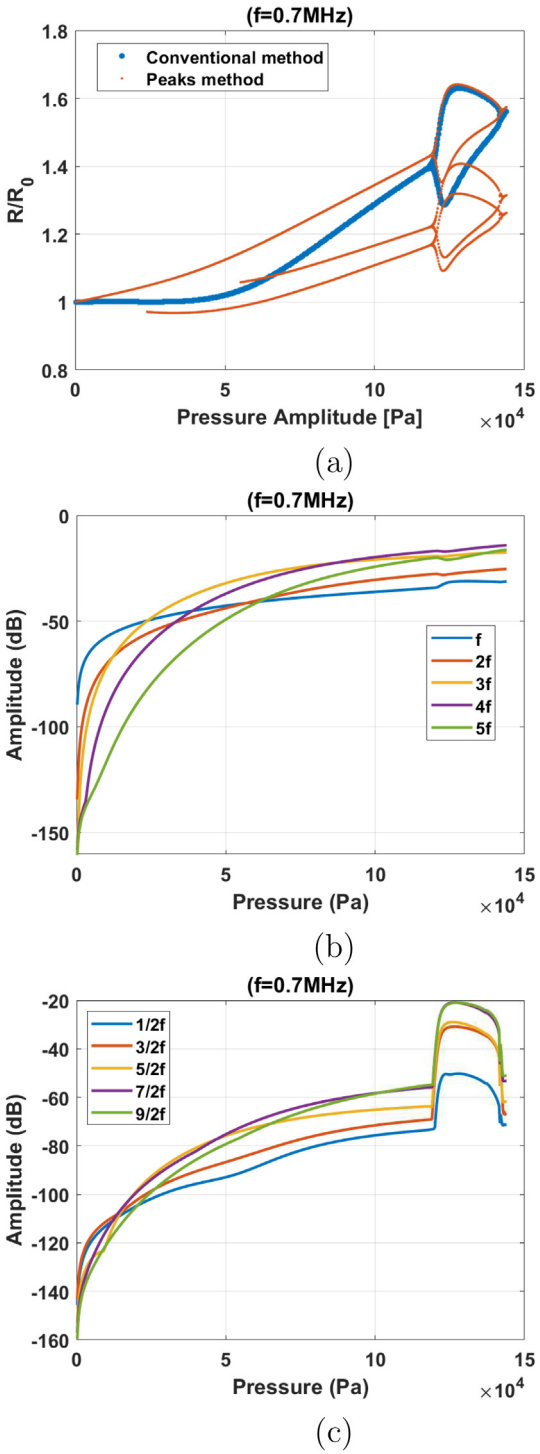

Fig. 7. a) Bifurcation structure of the normalized radial oscillations versus acoustic pressure of a 4 micron air bubble immersed in water as constructed by the conventional method (blue) and the peaks method (red) when f = 0.7 MHz, b) harmonics of the backscattered pressure versus acoustic pressure, c) SH and UH amplitudes of the backscattered pressure versus the acoustic pressure. (For interpretation of the references to colour in this figure legend, the reader is referred to the web version of this article.)

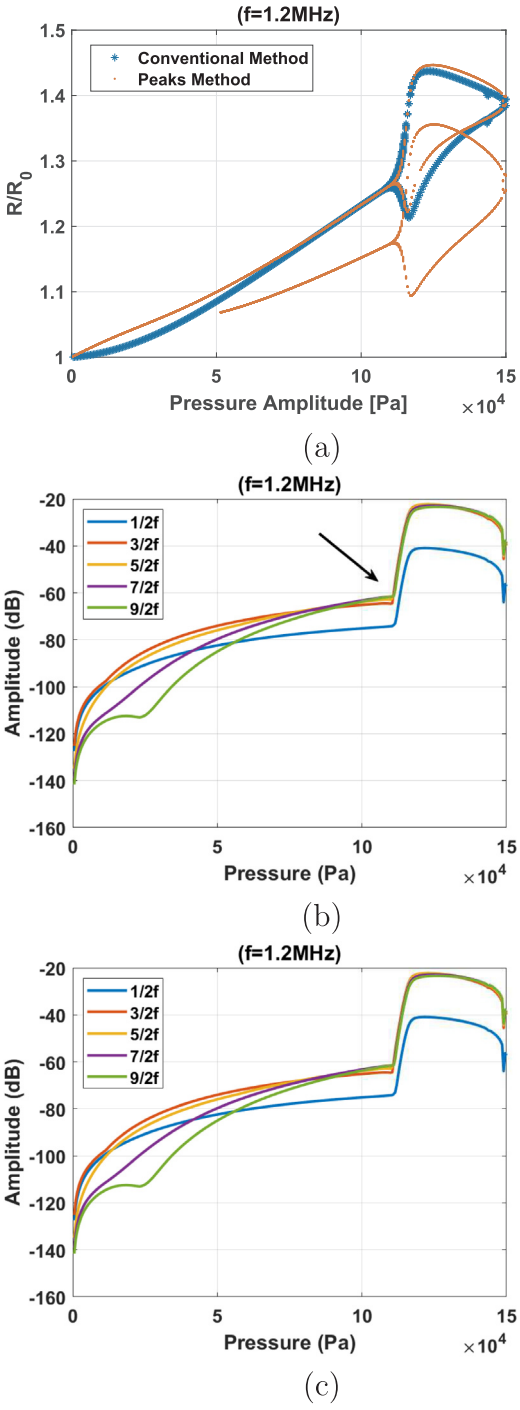

Fig. 8. a) Bifurcation structure of the normalized radial oscillations versus acoustic pressure of a 4 micron air bubble immersed in water as constructed by the conventional method (blue) and the peaks method (red) when f = 1.2 MHz, b) harmonics of the backscattered pressure versus acoustic pressure, c) SH and UH amplitudes of the backscattered pressure versus the acoustic pressure. (For interpretation of the references to colour in this figure legend, the reader is referred to the web version of this article.)

around and below resonance it was the conventional method that failed to reveal the intricate oscillation details. We conclude that for a comprehensive analysis of the bubble dynamics the two methods should be employed in tandem and the analysis will be incomplete in case that only one of the methods is used.

4. Discussion and summary

We have shown that the conventional method of generating bifurcation diagrams cannot reveal the hidden details of the oscillations that typically result in UH and SuH resonance. We have introduced a simple alternative method to generate the bifurcation diagrams; the method extracts the peaks of the oscillations and plots it as a function of

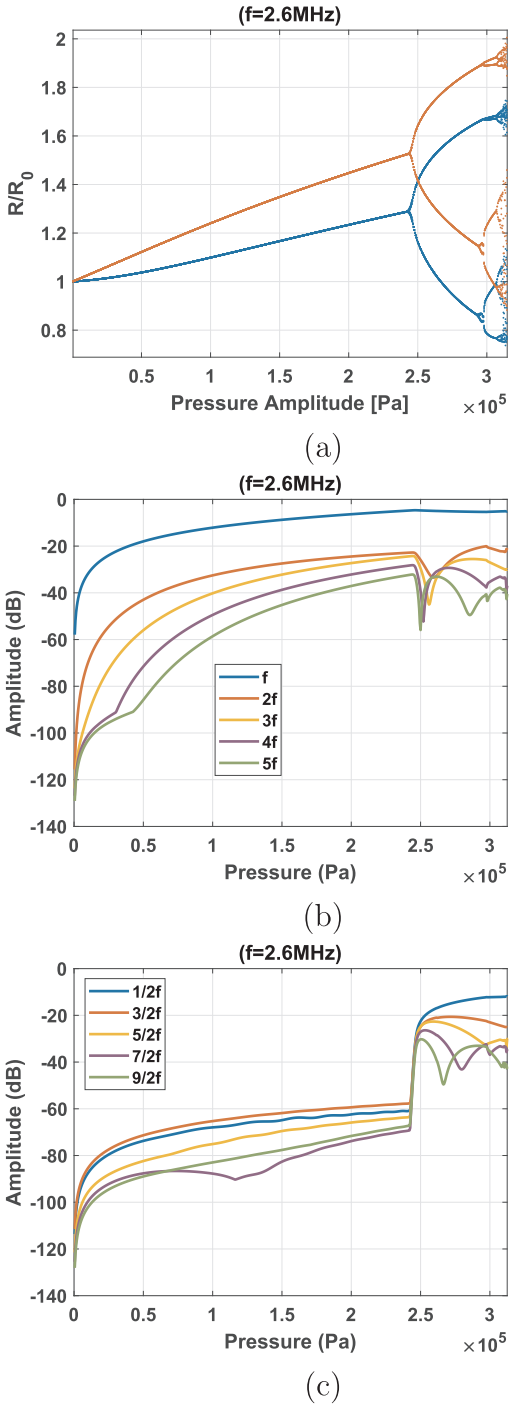

Fig. 9. a) Bifurcation structure of the normalized radial oscillations versus acoustic pressure of a 4 micron air bubble immersed in water as constructed by the conventional method (blue) and the peaks method (red) when f = 2.6 MHz, b) harmonics of the backscattered pressure versus acoustic pressure, c) SH and UH amplitudes of the backscattered pressure versus the acoustic pressure. (For interpretation of the references to colour in this figure legend, the reader is referred to the web version of this article.)

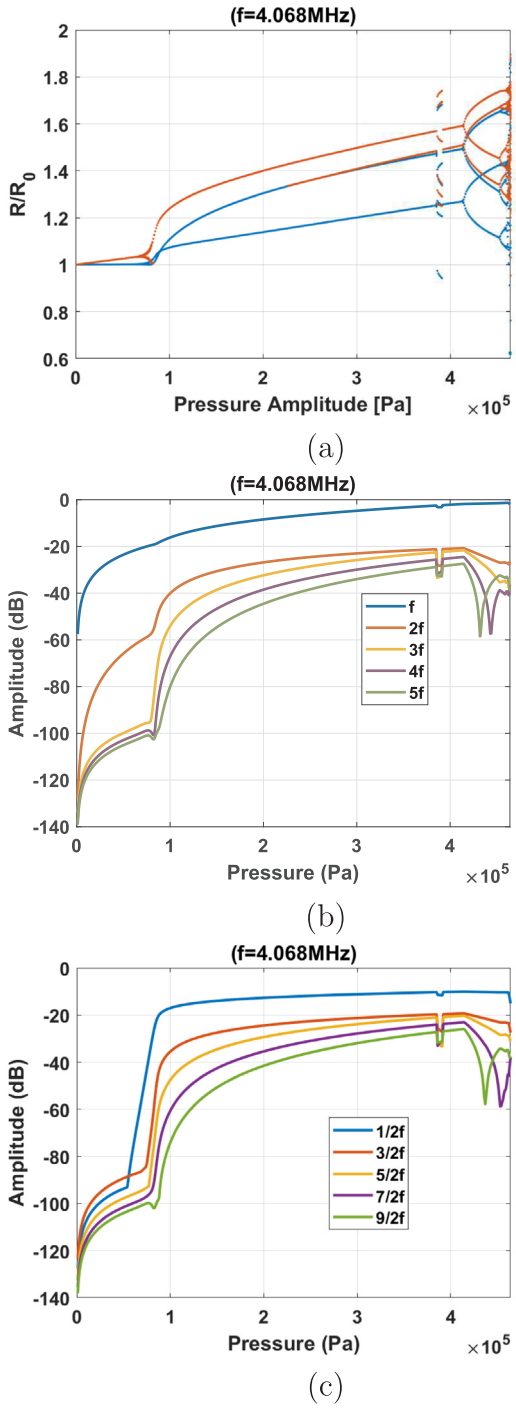

Fig. 10. a) Bifurcation structure of the normalized radial oscillations versus acoustic pressure of a 4 micron air bubble immersed in water as constructed by the conventional method (blue) and the peaks method (red) when f = 4.068 MHz, b) harmonics of the backscattered pressure versus acoustic pressure, c) SH and UH amplitudes of the backscattered pressure versus the acoustic pressure. (For interpretation of the references to colour in this figure legend, the reader is referred to the web version of this article.)

the given control parameter. When this method is applied alongside the conventional method one can reveal hidden details of the bubble oscillations and identify the parameter ranges where SuH, UH or SH oscillations occur. We can briefly categorize the scenarios shown in this paper as follows:

(1) The conventional method depicts a P1 oscillation regime, and the maxima method only reveals one maximum. In this case, the oscillation has a P1 resonance and the fundamental frequency component is the strongest in the backscattered signal. $\frac{1}{2}$ order SH and UHs are generated concomitant with PD in both graphs (constructed by conventional method and method of maxima) and $\frac{1}{2}$ order SHs, or $\frac{3}{2}$ UHs are stronger than other UHs.

(2) The conventional method depicts a P1 oscillation regime, but

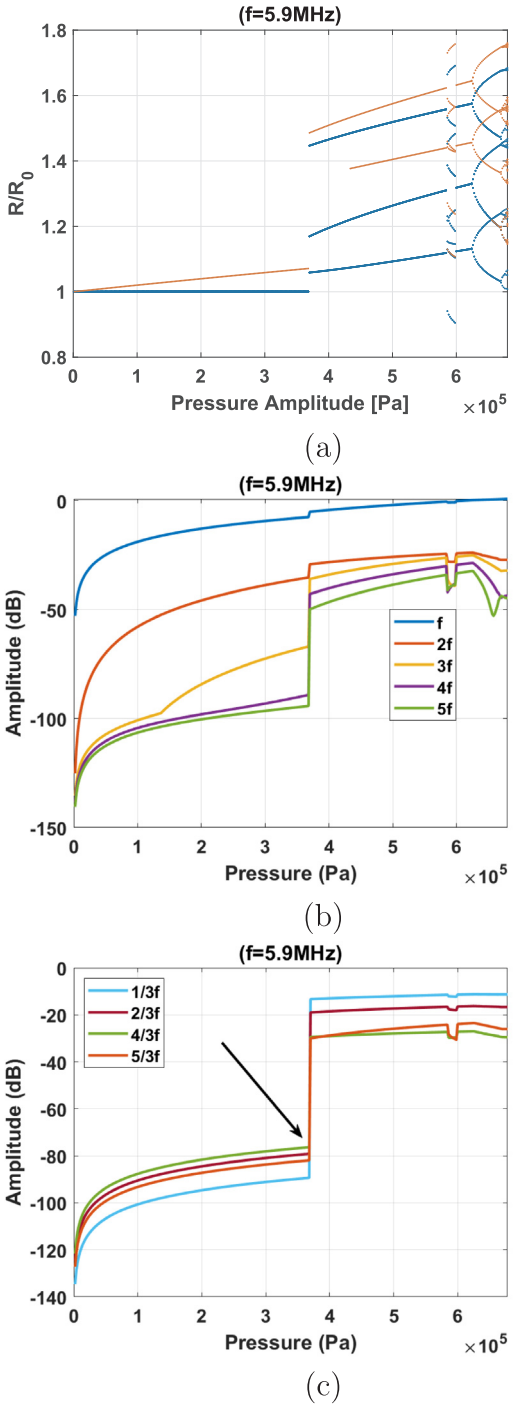

Fig. 11. a) Bifurcation structure of the normalized radial oscillations versus acoustic pressure of a 4 micron air bubble immersed in water as constructed by the conventional method (blue) and the peaks method (red) when f = 5.9 MHz, b) harmonics of the backscattered pressure versus acoustic pressure, c) SH and UH amplitudes of the backscattered pressure versus the acoustic pressure. (For interpretation of the references to colour in this figure legend, the reader is referred to the web version of this article.)

maxima method reveals n = 2,3,…maxima. In this case, the n-th order SuH frequency component is the strongest in the backscattered signal. Generation of PD in the conventional method is concomitant with the generation of n-PDs in the diagram constructed by the peaks method; this correlates with an UH resonance behavior of $\frac{(2n-1)}{2}$ or $\frac{(2n+1)}{2}$; in other words, these UHs are stronger than the $\frac{1}{2}$ order SHs and other UHs.

(3) The conventional method depicts a P2 oscillation regime, but the maxima method reveals only 1 maximum; in this case, we have a P2 resonance; $\frac{1}{2}$ order SH frequency component is the stronger than UHs.
(4) UH and SHs only exist when the conventional method predicts a P2 oscillations; however, the method of maxima needs to be applied alongside of traditional method to determine whether SH or UH resonance are present, as well as the order of UHs.

Heat and mass transfer across the bubble influence the dynamics of the bubble oscillations [48–52]. Heat and mass transfer in turn are nonlinear and depend on the nonlinear dynamics of the bubble. Since the main purpose of this paper was to introduce a simple and more comprehensive method to identify the SuH and UH oscillations of the bubble, for simplicity, the effects of heat and mass transfer were neglected. Nonlinear dynamics of heat and mass transfer requires further investigation and is beyond the scope of this paper. However, for accurate optimization of the applications and understanding of the associated phenomena with bubble dynamics, these effects must be considered.

Detailed studies on the effect of initial conditions (ICs) (R(0) and $\dot{R}(0)$) on the dynamical evolution of the bubble oscillations [28–34] have resulted in the discovery of new nonlinear features [29–34]. For example, depending on the ICs, the bubble has shown to exhibit period 1 (P1), P2 or P3 oscillations [31,33]. Application of the method proposed in this paper can help to better understand and categorize these nonlinear features, especially in the SuH and UH oscillation regimes. These results may be used to optimize applications by sending the proper pre-conditioning pulses to manipulate the ICs of the bubble to achieve the desirable behavior.

In contrast enhanced ultrasound imaging SH component of the backscattered signal is used to enhance the contrast to tissue ratio since the tissue does not produce SHs and UHs [53]. UHs oscillations, however have the advantage of generating images with higher resolution due to higher frequency [53]. Understating the ultrasound exposure parameters for the generation and enhancement of UHs will help to acquire images with high contrast to tissue ratio and resolution. Preconditioning pulses may help in enhancing the UH signal and using the methods described in this work can help in identification of optimum pre-conditioning pulses to enhance UHs. Another important application of bubbles in medicine is in molecular acoustic angiography [54] where the high frequency response of the bubbles is used to acquire images with superior resolution. In this regard higher order SuHs [54,55] or higher order UHs can be used to achieve high contrast and high resolution due to higher frequency response of the bubbles. Due to the lack of tissue SuHs and significant UHs only the bubble response is detected and micro-vessels can be visualized with superior detail and resolution. Identification of the exposure parameters for the SuH and UH responses of the bubbles can be used in these applications.

The nonlinear behavior of the lipid shell enhances the generation of SHs $\left(\frac{1}{2}, \frac{1}{3}, \frac{2}{3}, \frac{1}{4}, \frac{3}{4}\cdots\right)$ at very low acoustic pressures and over a more extensive frequency range [56,57]. The behavior of lipid shell MBs are more complex due to the nonlinear response of the encapsulating shell. For example the buckling of the lipid shell can result in compression only behavior [58]. Implementation of the proposed method in this paper can shine a brighter light on the behavior of lipid coated MBs. Our proposed approach can be used to optimize the wide range of applications that employ lipid coated MBs (for example: blood brain barrier opening [59], UH imaging [53], SuH imaging [54,55], Passive acoustic Imaging [60] and treatment monitoring [61]). The pressure radiated by the SuHs is attenuated much faster due to the higher attenuation of the higher harmonics [62,63]. This property can be used to enhance the heat deposition in therapeutic applications of ultrasound [62,63] especially for thermal therapy in regions with higher blood perfusion or tissue located beyond an obstacle like bone where delivery

of acoustic energy is limited. Furthermore, SuH oscillations may result in better mixing; identification of the relative frequencies and pressures can help in setting up a specific shape oscillation to increase the efficacy of these applications. Furthermore, the anatomy of the giant resonances [4] and their nonlinear properties can be studied with more detail; the lower bound of frequency to create a desired giant resonance can be identified. Since knowledge of the bifurcation structure is critical for non-feedback techniques [30] to control the multi-stability of the bubble system a more detailed understanding of the system bifurcation structure can be helpful in such control techniques by identifying the proper exposure parameters.

Acknowledgments

The work is supported by the Natural Sciences and Engineering Research Council of Canada (Discovery Grant RGPIN-2017-06496), NSERC and the Canadian Institutes of Health Research (Collaborative Health Research Projects) and the Terry Fox New Frontiers Program Project Grant in Ultrasound and MRI for Cancer Therapy (project #1034). A.J. Sojahrood is supported by a CIHR Vanier Scholarship.

References

[1] U. Parlitz, et al., Bifurcation structure of bubble oscillators, J. Acoust. Soc. Am. 88 (1990) 1061–1077.
[2] A. Prosperetti, L.A. Crum, K.W. Commander, Nonlinear bubble dynamics, J. Acoust. Soc. Am. 83 (1988) 502–514.
[3] T.G. Leighton, The Acoustic Bubble, Academic press, 2012.
[4] W. Lauterborn, T. Kurz, Physics of bubble oscillations, Rep. Progr. Phys. 73 (2010) 106501.
[5] W. Lauterborn, U. Parlitz, Methods of chaos physics and their application to acoustics, J. Acoust. Soc. Am. 84 (1988) 1975–1993.
[6] W. Lauterborn, E. Cramer, Subharmonic route to chaos observed in acoustics, Phys. Rev. Lett. 47 (1981) 1445.
[7] W. Lauterborn, J. Holzfuss, Acoustic chaos, Int. J. Bifurcation Chaos 1 (1991) 13–26.
[8] A. Prosperetti, A. Lezzi, Bubble dynamics in a compressible liquid. Part 1. First-order theory, J. Fluid Mech. 168 (1986) 457–478.
[9] L. Hoff, Acoustic Characterization of Contrast Agents for Medical Ultrasound Imaging, Springer Science & Business Media, 2001.
[10] S.M. van der Meer, et al., Microbubble spectroscopy of ultrasound contrast agents, J. Acoust. Soc. Am. 121 (2007) 648–656.
[11] A. Muthupandian, et al., Bubbles in an acoustic field: an overview, Ultrason. Sonochem. 14 (2007) 470–475.
[12] T.G. Leighton, From seas to surgeries, from babbling brooks to baby scans: the acoustics of gas bubbles in liquids, Int. J. Mod. Phys. B 18 (25) (2004) 3267–3314.
[13] K.S. Suslick, Sonochemistry, science 247 (1990) 1439–1445.
[14] B.D. Storey, A.J. Szeri, Water vapour, sonoluminescence and sonochemistry, Proc. R. Soc. London A: Mat. Phys. Eng. Sci. 456 (1999) (2000) Royal Society.
[15] L. Crum, et al. (Ed.), Sonochemistry and Sonoluminescence, Vol. 524 Springer Science & Business Media, 2013.
[16] K. Yasui, et al., Theoretical study of single-bubble sonochemistry, J. Chem. Phys. 122 (2005) 224706.
[17] H. Lais, et al., Numerical modelling of acoustic pressure fields to optimize the ultrasonic cleaning technique for cylinders, Ultrason. Sonochem. 45 (2018) 7–16.
[18] T. Segers, et al., Monodisperse versus polydisperse ultrasound contrast agents: non-linear response, sensitivity, and deep tissue imaging potential, Ultrasound Med. Biol. 44 (2018) 1482–1492.
[19] K.J. Haworth, et al., Passive imaging with pulsed ultrasound insonations, J. Acoust. Soc. Am. 132 (1) (2012) 544–553.
[20] K. Ferrara, R. Pollard, M. Borden, Ultrasound microbubble contrast agents: fundamentals and application to gene and drug delivery, Annu. Rev. Biomed. Eng. 9 (2007) 415–447.
[21] M.A. OReilly, et al., Focused-ultrasound disruption of the blood-brain barrier using closely-timed short pulses: influence of sonication parameters and injection rate, Ultrasound Med. Biol. 37 (2011) 587–594.
[22] R.G. Holt, R.A. Roy, Measurements of bubble-enhanced heating from focused, MHz-frequency ultrasound in a tissue-mimicking material, Ultrasound Med. Biol. 27 (2001) 1399–1412.
[23] S. Yoshizawa, et al., High intensity focused ultrasound lithotripsy with cavitating microbubbles, Med. Biol. Eng. Comput. 47 (2009) 851–860.
[24] K.B. Bader, K.J. Haworth, H. Shekhar, A.D. Maxwell, T. Peng, D.D. McPherson, C.K. Holland, Efficacy of histotripsy combined with rt-PA in vitro, Phys. Med. Biol. 61 (2016) 5253.
[25] A.J. Sojahrood, M.C. Kolios, Classification of the nonlinear dynamics and bifurcation structure of ultrasound contrast agents excited at higher multiples of their resonance frequency, Phys. Lett. A 376 (2012) 2222–2229.
[26] S. Behnia, A.J. Sojahrood, W. Soltanpoor, O. Jahanbakhsh, Suppressing chaotic oscillations of a spherical cavitation bubble through applying a periodic perturbation, Ultrasonics Sonochem. 16 (2009) 502–511.
[27] A.J. Sojahrood, et al., Influence of the pressure-dependent resonance frequency on the bifurcation structure and backscattered pressure of ultrasound contrast agents: a numerical investigation, Nonlinear Dyn. 80 (2015) 889–904.
[28] S. Behnia, A.J. Sojahrood, W. Soltanpoor, L. Sarkhosh, Towards classification of the bifurcation structure of a spherical cavitation bubble, Ultrasonics 49 (8) (2009) 605–610.
[29] F. Hegedűs, L. Kullmann, Basins of attraction in a harmonically excited spherical bubble model, Periodica Polytechnica Mech. Eng. 56 (2012) 125–132.
[30] F. Hegedűs, et al., Non-feedback technique to directly control multistability in nonlinear oscillators by dual-frequency driving, Nonlinear Dyn. (2018) 1–21.
[31] F. Hegedűs, C. Kalmár, Dynamic stabilization of an asymmetric nonlinear bubble oscillator, Nonlinear Dyn. (2018) 1–18.
[32] F. Hegedűs, Topological analysis of the periodic structures in a harmonically driven bubble oscillator near Blake's critical threshold: Infinite sequence of two-sided Farey ordering trees, Phys. Lett. A 380–10 (2016) 1012–1022.
[33] R. Varga, F. Hegedűs, Classification of the bifurcation structure of a periodically driven gas bubble, Nonlinear Dyn. 86 (2016) 1239–1248.
[34] F. Hegedűs, C. Hős, L. Kullmann, Stable period 1, 2 and 3 structures of the harmonically excited Rayleigh-Plesset equation applying low ambient pressure, IMA J. Appl. Math. 78 (2012) 1179–1195.
[35] Y. Zhang, Chaotic oscillations of gas bubbles under dual-frequency acoustic excitation, Ultrasonics Sonochem. 40 (2018) 151–157.
[36] Y. Zhang, Y. Gao, X. Du, Stability mechanisms of oscillating vapor bubbles in acoustic fields, Ultrasonics Sonochem. 40 (2018) 808–814.
[37] Y. Zhang, S. Li, Bubble dynamics under acoustic excitation with multiple frequencies, 72 IOP Publishing, 2015No. 1.
[38] Y. Zhang, Y. Zhang, S. Li, Combination and simultaneous resonances of gas bubbles oscillating in liquids under dual-frequency acoustic excitation, Ultrasonics Sonochem. 35 (2017) 431–439.
[39] S.A. Suslov, A. Ooi, R. Manasseh, Nonlinear dynamic behavior of microscopic bubbles near a rigid wall, Phys. Rev. E 85 (2012) 066309.
[40] F. Dzaharudin, A. Ooi, R. Manasseh, Effects of boundary proximity on mono-dispersed microbubbles in ultrasonic fields, J. Sound Vib. 410 (2017) 330–343.
[41] F. Dzaharudin, S.A. Suslov, R. Manasseh, A. Ooi, Effects of coupling, bubble size, and spatial arrangement on chaotic dynamics of microbubble cluster in ultrasonic fields, J. Acoust. Soc. Am. 134 (2013) 3425–3434.
[42] K. Klapcsik, F. Hegedűs, The effect of high viscosity on the collapse-like chaotic and regular periodic oscillations of a harmonically excited gas bubble, Ultrasonics Sonochem. 27 (2015) 153–164.
[43] F. Hegedűs, K. Klapcsik, The effect of high viscosity on the evolution of the bifurcation set of a periodically excited gas bubble, Chaos, Solitons Fract. 104 (2017) 198–208.
[44] K. Klapcsik, R. Varga, F. Hegedűs, Bi-parametric topology of subharmonics of an asymmetric bubble oscillator at high dissipation rate, Nonlinear Dyn. (2018) 1–17, https://doi.org/10.1007/s11071-018-4497-2.
[45] J.B. Keller, M. Miksis, Bubble oscillations of large amplitude, J. Acoust. Soc. Am. 68 (1980) 628–633.
[46] S. Hilgenfeldt, D. Lohse, M. Zomack, Sound scattering and localized heat deposition of pulse-driven microbubbles, J. Acoust. Soc. Am. 107 (2000) 3530–3539.
[47] Y. Zhang, A generalized equation for scattering cross section of spherical gas bubbles oscillating in liquids under acoustic excitation, J. Fluids Eng. 135 (9) (2013) 091301.
[48] Y. Zhang, Heat transfer across interfaces of oscillating gas bubbles in liquids under acoustic excitation, Int. Commun. Heat Mass Transfer 43 (2013) 1–7.
[49] Y. Zhang, Y. Gao, Z. Guo, X. Du, Effects of mass transfer on damping mechanisms of vapor bubbles oscillating in liquids, Ultrasonics Sonochem. 40 (2018) 120–127.
[50] F. Hegedűs, C. Hos, L. Kullmann, Influence of heat transfer on the dynamic response of a spherical gas/vapour bubble, Int. J. Heat Fluid Flow 31 (6) (2010) 1040–1049.
[51] A. Prosperetti, The thermal behaviour of oscillating gas bubbles, J. Fluid Mech. 222 (1991) 587–616.
[52] A. Prosperetti, L.A. Crum, K.W. Commander, Nonlinear bubble dynamics, J. Acoust. Soc. Am. 83 (2) (1988) 502–514.
[53] V. Daeichin, et al., Subharmonic, non-linear fundamental and ultraharmonic imaging of microbubble contrast at high frequencies, Ultrasound Med. Biol. 41 (2015) 486–497.
[54] S.E. Shelton, et al., Molecular acoustic angiography: a new technique for high-resolution superharmonic ultrasound molecular imaging, Ultrasound Med. Biol. 42 (2016) 769–781.
[55] A. Bouakaz, et al., Super harmonic imaging: a new imaging technique for improved contrast detection, Ultrasound Med. Biol. 28 (2002) 59–68.
[56] A.J Sojahrood, R. Karshafian, M.C. Kolios, Bifurcation structure of the ultrasonically excited microbubbles undergoing buckling and rupture, in: proceedings of Meetings on Acoustics ICA 2013. Vol. 19. No. 1. ASA, 2013.
[57] A.J. Sojahrood, R. Karshafian, M.C. Kolios, Detection and characterization of higher order nonlinearities in the oscillations of Definity at higher frequencies and very low acoustic pressures, Ultrasonics Symposium (IUS), 2012 IEEE International, IEEE, 2012.
[58] P. Marmottant, S. van der Meer, M. Emmer, M. Versluis, N. de Jong, S. Hilgenfeldt, D. Lohse, A model for large amplitude oscillations of coated bubbles accounting for buckling and rupture, J. Acoust. Soc. Am. 118 (6) (2005) 3499–3505.
[59] M.A. OReilly, K. Hynynen, Blood-brain barrier: real-time feedback-controlled focused ultrasound disruption by using an acoustic emissions-based controller, Radiology 263 (2012) 96106.
[60] K.J. Haworth, et al., Passive imaging with pulsed ultrasound insonations, J. Acoust. Soc. Am. 132 (1) (2012) 544–553.

[61] C.C. Coussios, et al., Role of acoustic cavitation in the delivery and monitoring of cancer treatment by high-intensity focused ultrasound (HIFU), Int. J. Hyperth. 23 (2) (2007) 105–120.
[62] R.G. Holt, R.A. Roy, Measurements of bubble-enhanced heating from focused, MHz-frequency ultrasound in a tissue-mimicking material, Ultrasound Med. Biol. 27 (10) (2001) 1399–1412.
[63] A.J. Sojahrood, M.C. Kolios, The utilization of the bubble pressure dependent harmonic resonance frequency for enhanced heating during high intensity focused ultrasound treatments, in: AIP Conference Proceedings (Vol. 1481, No. 1, (2012, October) pp. 345–350). AIP.